



Contents lists available at ScienceDirect

Manufacturing Letters

journal homepage: www.elsevier.com/locate/mfglet

Letters

Toward determining melt pool quality metrics via coaxial monitoring in laser powder bed fusion

Brian A. Fisher^{a,*}, Brandon Lane^b, Ho Yeung^b, Jack Beuth^a^a NextManufacturing Center, Carnegie Mellon University, Pittsburgh, PA, United States^b Intelligent Systems Division, National Institute of Standards and Technology, Gaithersburg, MD, United States

ARTICLE INFO

Article history:

Received 15 September 2017

Received in revised form 6 February 2018

Accepted 10 February 2018

Available online xxxxx

Keywords:

Additive manufacturing

Melt pool monitoring

Coaxial monitoring

Laser powder bed fusion

NIST Additive Manufacturing Metrology

Testbed (AMMT)

ABSTRACT

The current industry trend in metal additive manufacturing is towards greater real time process monitoring capabilities during builds to ensure high quality parts. While the hardware implementations that allow for real time monitoring of the melt pool have advanced significantly, the knowledge required to correlate the generated data to useful metrics of interest are still lacking. This research presents promising results that aim to bridge this knowledge gap by determining a novel means to correlate easily obtainable sensor data (thermal emission) to key melt pool size metrics (e.g., melt pool cross sectional area).

© 2018 Society of Manufacturing Engineers (SME). Published by Elsevier Ltd. All rights reserved.

1. Introduction

The implementation of tools to monitor the melt pool in metal additive manufacturing (AM) processes is widely considered essential to the adoption of those processes for advanced component production [1]. The fusion process is so variable that even when nominal deposition parameters are implemented, flaws in the resultant part are possible [2,3], making it essential to monitor the process on the length and time scales needed to detect flaws. Laser powder bed fusion (LPBF) is particularly difficult to monitor because of the small length scales, with melt pools roughly 50 μm to 250 μm wide [4], and short time scales, with melt pool phenomena occurring over roughly 10 μs to 100 μs [3,5]. The most promising solution to reliably obtain melt pool scale information in the LPBF process is to align sensors along the optical path of the laser [6–8]. In doing so, spatial coordination of the sensors with the melt pool is guaranteed, allowing for more targeted data collection.

The majority of melt pool monitoring tools that are commercially available utilize this coaxial monitoring technique [9–11]. The current hardware is capable of recording copious amounts of data; however, the associated software packages rely on the user

to draw their own conclusions from those data. Picking out anomalies or even understanding what information is important to consider is difficult without an informed framework that ties sensor outputs to part quality metrics. The current research aims to bridge this knowledge gap by presenting a means to correlate readily obtainable sensor data (thermal emission) to key melt pool size metrics (e.g., melt pool cross sectional area). This correlation does not rely on information about the melt pool geometry, as has prior research [8,12], but instead looks only at the total in-band thermal emission from each melt pool (further called “emission”).

2. Methods

Experiments were performed on the prototyping system (Fig. 1) developed by the National Institute of Standards and Technology (NIST), a precursor to NIST’s current Additive Manufacturing Metrology Testbed (AMMT) [13,14]. The only notable modifications to the prototyping testbed were the addition of a hot plate within the argon purge box and thermocouples welded to the experiment plates. The material used in this research is Ti-6Al-4V due to its popularity within the AM community [15].

A series of single bead, beam-on-plate experiments was conducted at a wide range of plate temperatures, beam powers, and beam velocities to generate a dense matrix of melt pools that span the practical process parameter range of the AMMT prototyping system. The thermal emission from each melt pool was imaged

* Corresponding author at: 5000 Forbes Ave., Scaife Hall, Pittsburgh, PA 15213, United States.

E-mail address: brianfis@andrew.cmu.edu (B.A. Fisher).

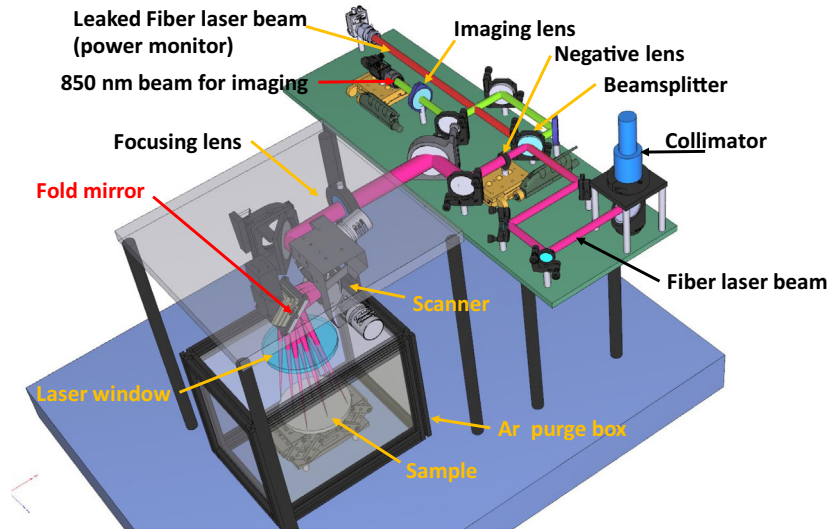


Fig. 1. A schematic of the AMMT prototyping system used in this research, courtesy of Lane et al. [14].

by a high speed digital camera with a monochrome, 12 bit detector and an $850 \text{ nm} \pm 20 \text{ nm}$ optical filter. A frame rate of 50 kHz and an integration time of $0.5 \mu\text{s}$ (set such that the camera images do not saturate) was used for data collection. While no rigorous calculation of the spatial resolution of the camera system was yet completed [16], the instantaneous field of view of each pixel was measured at approximately $15 \mu\text{m} \times 15 \mu\text{m}$. All camera settings were held constant for all data collected. An example melt pool top view image, cross sectional area image, and thermal emission image can be seen in Fig. 2.

Emission was determined by adding up the values of all pixels above a threshold of 20 (reported in “digital level”, or DL) in the camera images and averaging over the available images for that scan track. Therefore, all information about the melt pool geometry from the emission data is lost. The threshold value was set 3σ above the average signal noise. After the experimental plate was removed from the LPBF machine, each scan track was cross sectioned normal to the track length and imaged to get the melt pool cross sectional area (area). To generate process maps of constant area or emission, experimental data taken at each plate temperature were piecewise linearly interpolated to find locations of a prescribed metric in power-velocity space [17]. Those interpolated locations are plotted in Figs. 3 and 4 as data points.

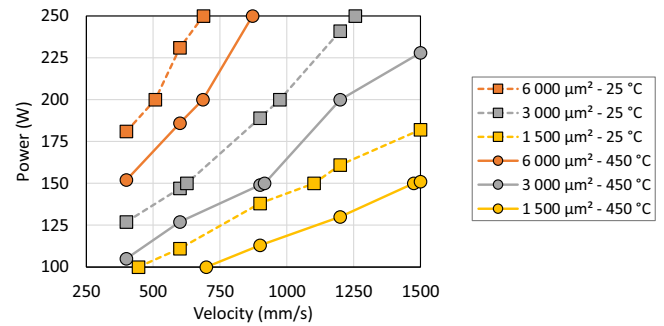


Fig. 3. Curves of constant melt pool cross-section area measured ex-situ.

3. Theory

When viewing thermal emission from a heat source, the relationship between camera signal and temperature will be highly nonlinear [18]. By analyzing the camera signal values directly instead of trying to convert those data to temperatures, the number of calibration steps needed to define the camera system are

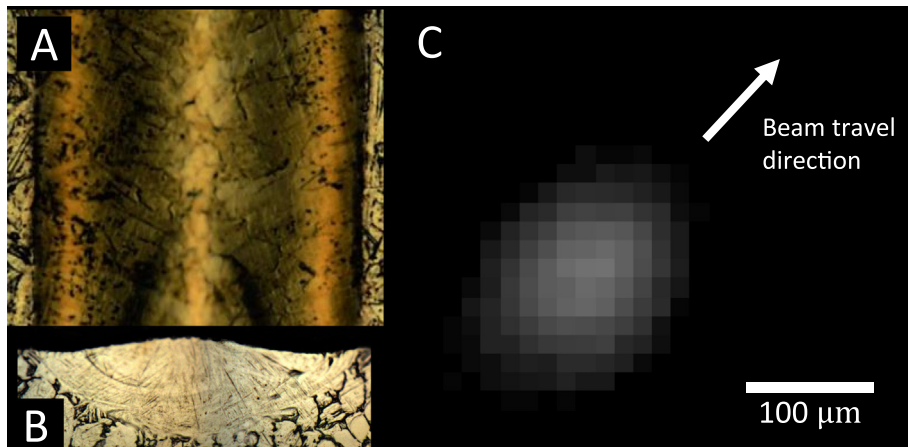


Fig. 2. All images are for the same scan track ($P = 250 \text{ W}$, $V = 600 \text{ mm/s}$, $T = 25 \text{ }^\circ\text{C}$) and at the same scale. (A) Microscope image of the top surface of the scan track. (B) Microscope image of the cross sectional melt pool area (sectioned, polished, and etched). (C) Example thermal emission image from the scan track.

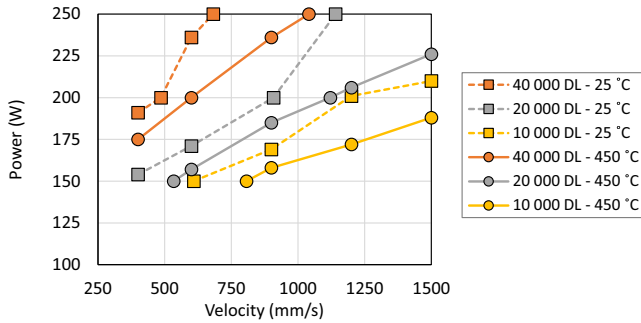


Fig. 4. Curves of constant melt pool emission obtained from in-situ melt pool images.

reduced [18]. The authors will show that though neither radiant nor absolute temperatures are known, the thermal information gathered from the camera system is still highly valuable for melt pool monitoring applications.

4. Results and discussion

The process map for area can be seen in Fig. 3, with the corresponding map for emission in Fig. 4. In both cases, it is clear from the slope of the curves of constant metric in power-velocity space as well as the shifts in those curves due to changes in plate temperature that all three parameters tested (power, velocity, and plate temperature) have significant effects on both area and emission. Furthermore, each successive curve constitutes a 2X decrease in the metric of interest, with the largest values chosen to start in similar locations in process space: 6 000 μm^2 at 25 °C in Fig. 3 and 40 000 DL at 25 °C in Fig. 4 (orange squares with dotted connecting lines).

The curves in Figs. 3 and 4 are similar, though with different magnitudes of process variable changes necessary to create the 2X jumps between curves. This means that correlations based on mapping of values between figures is possible, and therefore emission can be used as a metric for area, which is an important melt pool characteristic [19] that is nearly impossible to measure directly in-situ.

An example of a correlation that can be made is as follows. If power is held at 200 W and plate temperature is held at 25 °C, the curve of area vs. emission for the velocity range measured is linear with a slope of roughly 7 DL/ μm^2 .

5. Conclusions

Emission from the melt pool in LPBF has been shown to have similar trends to area. Both metrics vary with beam power, beam velocity, and plate temperature. The thermal information in this research was obtained with a high speed camera, but no spatial information was used in analyzing it, meaning that the thermal information could have been obtained by a simple photodiode. The multiple order of magnitude reduction in information generation by a photodiode as opposed to a camera detector

makes the implementation of the correlations found in this research applicable for real time feedback control systems.

Acknowledgements

This research was partially supported by NIST through the Pathways Program.

References

- [1] Tapia G, Elwany A. A review on process monitoring and control in metal-based additive manufacturing. *J Manuf Sci Eng* 2014;136. <https://doi.org/10.1115/1.4028540>.
- [2] Cunningham R, Narra SP, Montgomery C, Beuth J, Rollett AD. Synchrotron-based X-ray microtomography characterization of the effect of processing variables on porosity formation in laser power-bed additive manufacturing of Ti-6Al-4V. *JOM* 2017;69:479–84. <https://doi.org/10.1007/s11837-016-2234-1>.
- [3] Khairallah SA, Anderson AT, Rubenchik A, King WE. Laser powder-bed fusion additive manufacturing: Physics of complex melt flow and formation mechanisms of pores, spatter, and denudation zones. *Acta Mater* 2016;108:36–45. <https://doi.org/10.1016/j.actamat.2016.02.014>.
- [4] Gong H, Rafi K, Gu H, Starr T, Stucker B. Analysis of defect generation in Ti-6Al-4V parts made using powder bed fusion additive manufacturing processes. *Addit Manuf* 2014;1:87–98. <https://doi.org/10.1016/j.addma.2014.08.002>.
- [5] Zhao C, Fezzaa K, Cunningham RW, Wen H, De Carlo F, Chen L, et al. Real-time monitoring of laser powder bed fusion process using high-speed X-ray imaging and diffraction. *Sci Rep* 2017;7. <https://doi.org/10.1038/s41598-017-03761-2>.
- [6] Bardin F, Cobo A, Lopez-Higuera JM, Collin O, Aubry P, Dubois T, et al. Closed-loop power and focus control of laser welding for full-penetration monitoring. *Appl Opt* 2005;44:13–21.
- [7] Yadroitsev I, Krakhmalev P, Yadroitsava I. Selective laser melting of Ti6Al4V alloy for biomedical applications: Temperature monitoring and microstructural evolution. *J Alloys Compd* 2014;404–9. <https://doi.org/10.1016/j.jallcom.2013.08.183>.
- [8] Craeghs T, Clijsters S, Yasa E, Bechmann F, Berumen S, Kruth JP. Determination of geometrical factors in Layerwise Laser Melting using optical process monitoring. *Opt Lasers Eng* 2011;1440–6. <https://doi.org/10.1016/j.optlaseng.2011.06.016>.
- [9] Dunsky C. Process monitoring in laser additive manufacturing. *Ind Laser Solut* 2014. <http://www.industrial-lasers.com/articles/print/volume-29/issue-5/features/process-monitoring-in-laser-additive-manufacturing.html> (accessed July 17, 2017).
- [10] Toeppel T, Schumann P, Ebert M-C, Bokkes T, Funke K, Werner M, et al. 3D analysis in laser beam melting based on real-time process monitoring. *Mater Sci Technol Conf* 2016.
- [11] Nickels L. Improving the QA of 3D-printed parts. *Met Powder Rep* 2016;71:249–51. <https://doi.org/10.1016/j.mprp.2016.02.044>.
- [12] Heigel JC, Lane BM. Measurement of the melt pool length during single scan tracks in a commercial laser powder bed fusion process. *Int. Manuf. Sci. Eng. Conf. Proc.* Los Angeles, CA: ASME; 2017.
- [13] Vlasea ML, Lane B, Lopez F, Mekhontsev S, Donmez A. Development of powder bed fusion additive manufacturing test bed for enhanced real-time process control. *Solid Free Fabr Symp* 2015:527–39.
- [14] Lane B, Mekhontsev S, Grantham S, Vlasea ML, Whiting J, Yeung H, et al. Design, developments, and results from the NIST Additive Manufacturing Metrology Testbed (AMMT). *Solid Free Fabr Symp* 2016:1145–60.
- [15] Frazier WE. Metal additive manufacturing: a review. *J Mater Eng Perform* 2014;23:1917–28. <https://doi.org/10.1007/s11665-014-0958-z>.
- [16] Lane B, Grantham S, Yeung H, Zarobila C, Fox J. Performance characterization of process monitoring sensors on the NIST Additive Manufacturing Metrology Testbed. *Solid Free Fabr Symp* 2017.
- [17] Francis Z. The effects of laser and electron beam spot size in additive manufacturing processes. Carnegie Mellon University; 2017 [Doctoral Dissertation].
- [18] Lane B, Whinton EP. Calibration and measurement procedures for a high magnification thermal camera. *Natl Inst Stand Technol* 2015. <https://doi.org/10.6028/NIST.JR.8098>.
- [19] Gockel J, Beuth J, Taming K. Integrated control of solidification microstructure and melt pool dimensions in electron beam wire feed additive manufacturing of Ti-6Al-4V. *Addit Manuf* 2014;1–4:119–26. <https://doi.org/10.1016/j.addma.2014.09.004>.